Supplementary Material for:

Micro-Raman spectroscopy of lipid halo and dense-core amyloid plaques: aging process characterization in the Alzheimer's Disease APPswePS1ΔE9 mouse model

Emerson A. Fonseca[a,b,1,*], Lucas Lafetab[a,1], João Campos[a], Renan Cunha[a], Alexandre Barbosa[a,c], Marco A. Romano-Silva[d], Rafael Vieira[e], Leandro M. Malard[a], Ado Jorio[a,b]

[*]Corresponding author: fonseca.et.al@gmail.com
[1]These authors contributed equally to this work

This file includes:

S1. Table of the Molecular Vibrational Frequencies and Mode Assignments

| Frequency values (cm^{-1})	Assignments
418-429	cholesterol, cholesterol ester
702	cholesterol, cholesterol ester
719-725	sphingomyelin, C-N (membrane phospholipid head), symmetric stretch vibration of choline group, characteristic for phospholipids
763	ethanolamine group, phosphatidylethanolamine
782-791	cytosine/uracil ring breathing (nucleotide), phosphodiester bands in DNA, uracil, thymine, DNA: O P O, cytosine, pyrimidine
876	C-C-N+ symmetric stretching (lipids)
1007, 1022, 1033	phenylalanine (symmetric ring breathing), phenylalanine mode
1064-1069	skeletal C-C stretch of lipids, triglycerides (fatty acids)
1104	vibration (C-C), lipids, fatty acids
1090	phospholipids acyl chains
1131	fatty acid
1203-1263	amide III (β sheet) arising from coupling of C-N stretching and N-H
1267	C-H lipid, =C-H phospholipids
1272, 1286	unsaturated fatty acids, scissoring (=CH)
1295-1299	ceramide, palmitic acid, fatty acids, CH_2 deformation (lipid)
1302	fatty acid, phospholipids
1344	nucleic acid modes (DNA and RNA)
1384, 1427	unassigned mode
1428	lipid band, cholesteryl palmitate
1437	CH_2 deformation (lipid)
1446	CH_2 bending mode of proteins and lipids
1453	CH_2 deformation, protein band
1464	fatty acids, cholesterol, cholesterol ester
1494	DNA
1583	pyrimidine ring (nucleic acids)
1610-1614	cytosine (NH_2), Tyrosine, Phenylalanine
1660	amide I (C=O stretching) α-helix structure; (C-C) *cis*, lipids, fatty acids, C-C groups in unsaturated fatty acids
1670-1675	amide I (C=O stretching) β-sheet structure; cholesterol and its esters, (C-C) *trans*, lipids, fatty acids, ceramide
1681	glutamate, DNA unassigned mode
2727	C-H stretches
2843, 2850	CH_2 symmetric stretching of lipids (total lipids)
2880	CH_2 asymmetric stretching of lipids and proteins
2930-2935	CH_3 symmetric stretching of lipids and proteins
2947	C-H vibrations in lipids and proteins, asymmetric vibration CH_2, lipids, fatty acids
2952	CH_3 asymmetric stretching
2968	asymmetric vibration CH_2, lipids, fatty acids, cholesterol and cholesterol ester
2972	fatty acids
3016	CH_2 of lipids
070	amide B (NH stretching, resonant with amide II in β sheet), Fermi resonance

For more details, see references [1-3]
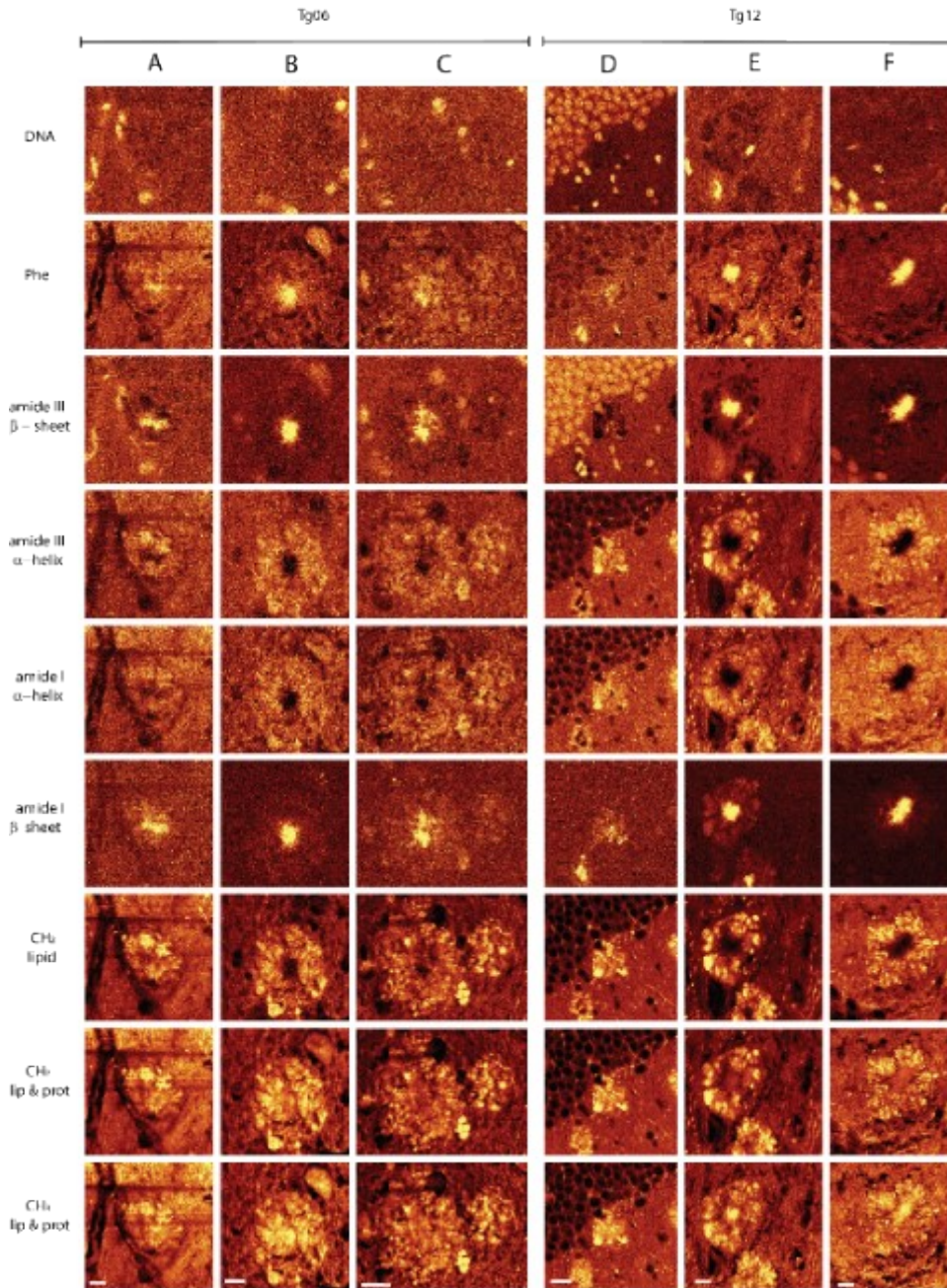
Fig. S1. High-spatial resolution hyperspectral images of 6 and 12-months old AD mice.
The images were generated by selecting filters for each frequency value in Project FIVE 5.0 WITec software. Main frequencies were able to identify in situ the core of the amyloid plaque: Phe (1007/10 cm^{-1}) amide III β sheet (centered at 1233/60 cm^{-1}), amide I β sheet (1670/10 cm^{-1}). CH$_2$ stretching of the total lipid (2850/10 cm^{-1}) forming the lipid halo, CH$_2$ stretching of the total lipid and protein (2880/10 cm^{-1}) and CH$_3$ stretching of the total lipid and protein (2930/10 cm^{-1}). Nuclei cells at DNA frequency (791/25 cm^{-1}). Note amide I and III α helix shows lipid halo structures as well, this is probably due to the overlapping frequencies of protein and lipid in these range (see frequencies table). CH$_2$ and CH$_3$ (2880/10 cm^{-1} and 2930/10 cm^{-1} respectively) frequencies related to protein and lipid stretching forms the lipid halo by also shown the amyloid plaque. In CH$_3$ frequency value, the contrast of the plaque is greater compared to CH$_2$ (2880 cm^{-1}). Scale bar, A-B, 10 μm; C-D, 20 μm; E-F, 10 μm. lip: lipid; prot: protein.

Principal Component Analysis

The determination of the number of components that will be used is made considering that the number of components must represent 90% of the data variance. Figure S2 presents the accumulated variance and the reference value of 92% as the minimum variance represented by the principal components.
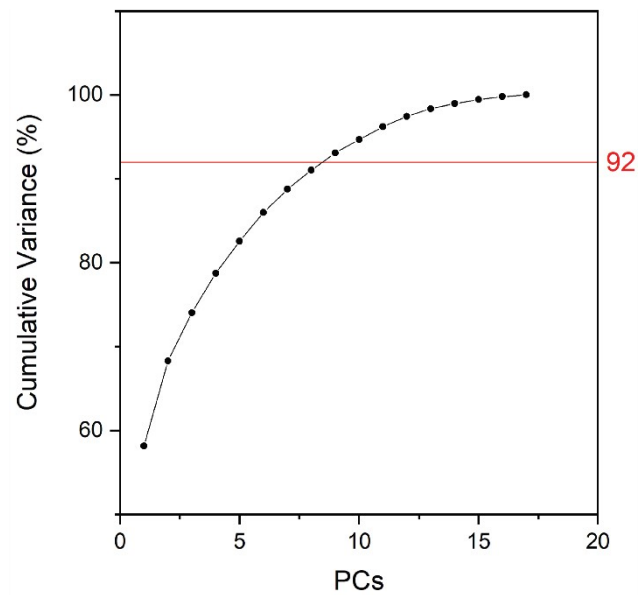

Fig. S2. Accumulated variance for each principal component.

Cluster Analysis

The determination of the number of clusters that will be used in the analysis is done using the variation of the total within-cluster mean square considering a certain number of clusters (Figure S3). The choice of the ideal value was made considering the number of clusters where there is a reduction in the variation of the values of the total within-cluster mean square.
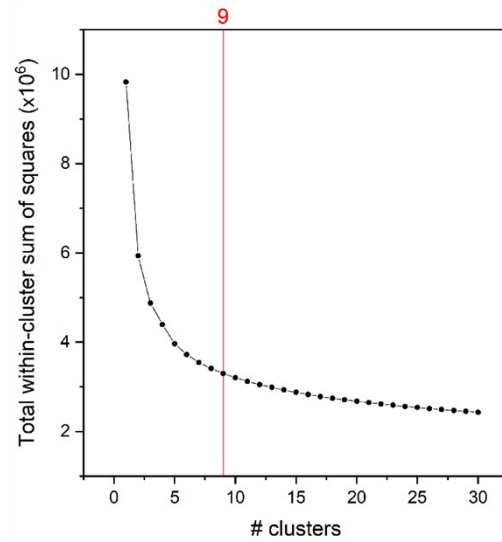

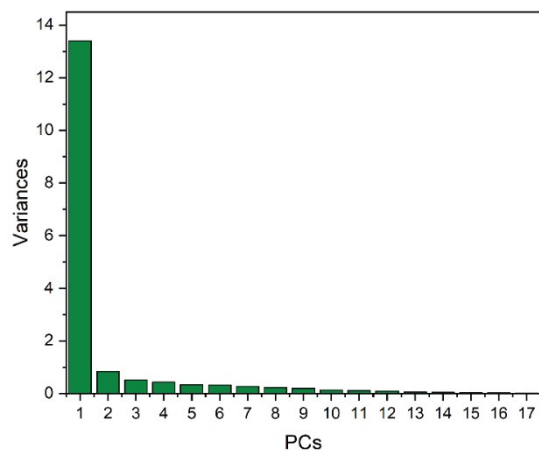Fig. S3. Variation of the total within-cluster mean square for each number of clusters.

Fig. S4. Screen plot showing the relevance of each PC to the data variance.
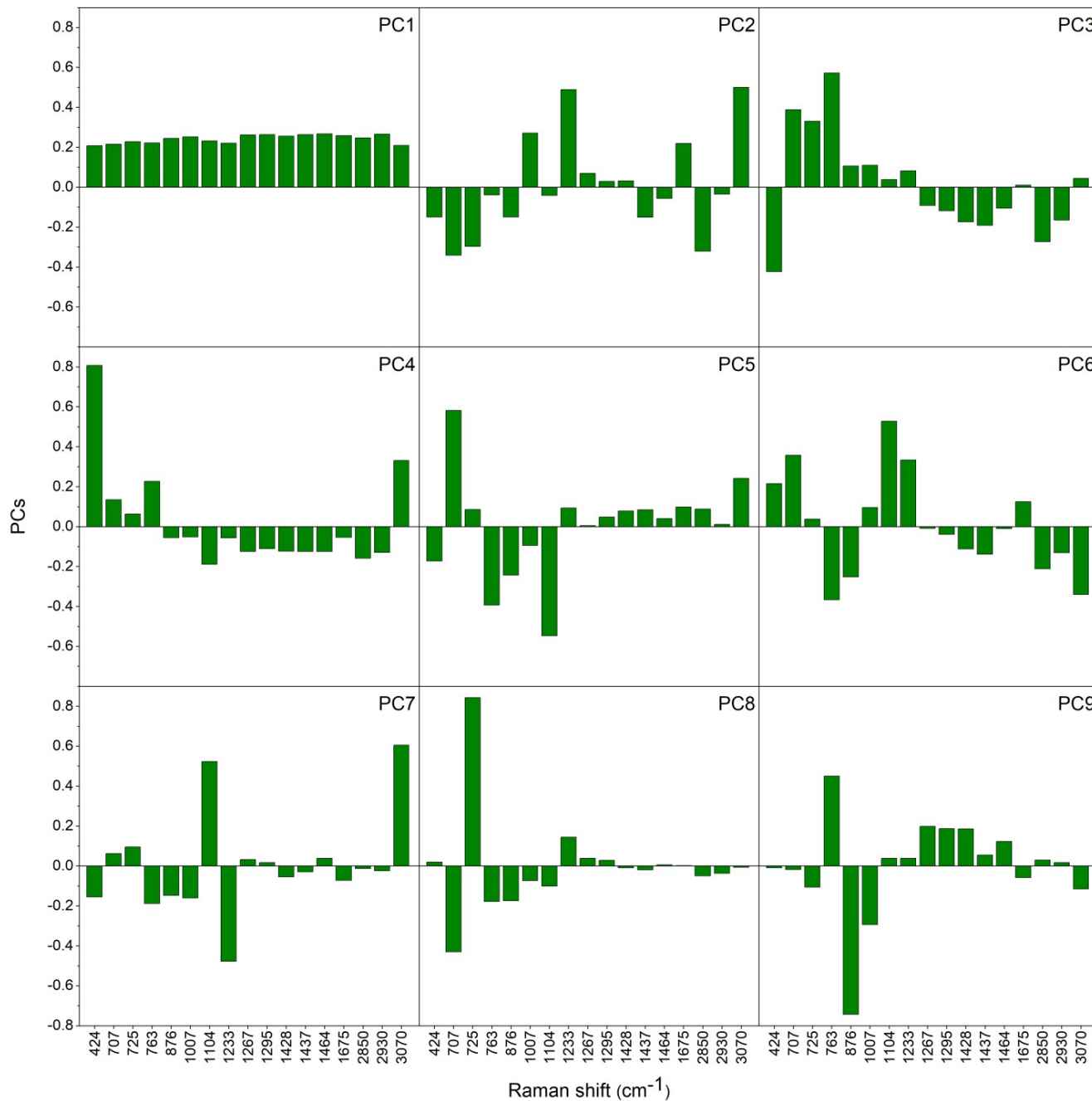
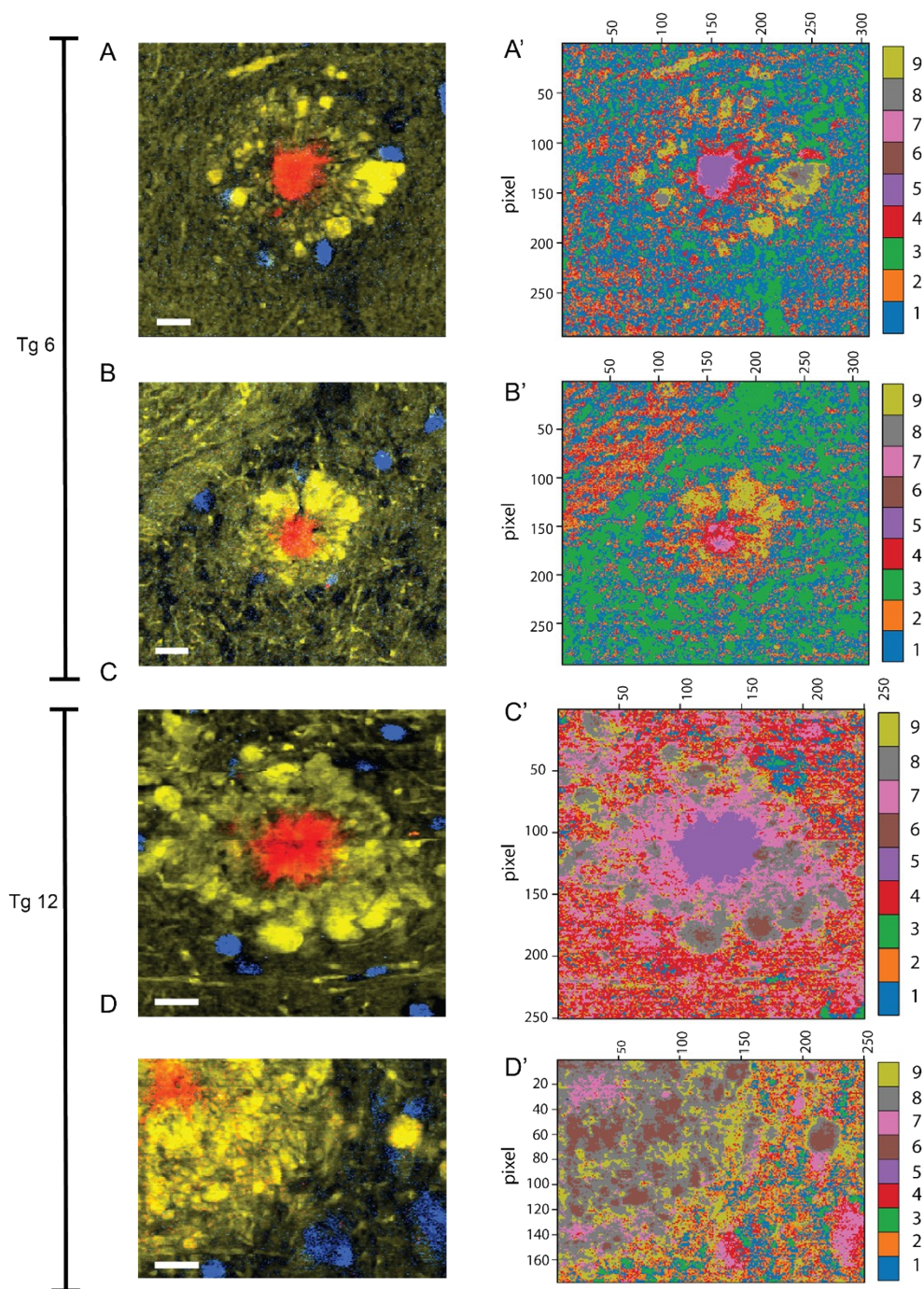Fig. S5. PC loadings for each of the nine PCs used for the cluster analysis.

Fig. S6. Cluster Maps of AD mice brain. On left column, hyperspectral Raman images (A-D), showing dense-core amyloid plaques (red), lipid (yellow) and DNA (blue). On right, cluster maps (A'-D'). Amyloid plaque is well defined in both young and aged mice by clusters 5 and 7. However, clusters 6 and 8 distribution is more pronounced in lipid halo of the Tg12 than Tg6. Scale bar 10 μm.

References

1.   A. Barth, C. Zscherp, Quarterly Reviews of Biophysics, 2002, 35, 369–430.
2.   K. Czamara, K. Majzner, M. Z. Pacia, K. Kochan, A. Kaczor, M. Baranska, Journal of Raman Spectroscopy, 2014, 46, 4–20.
     A. C. S. Talari, Z. Movasaghi, S. Rehman, I. U. Rehman, Applied Spectroscopy Reviews, 2015, 50, 46–111.